M. Alfano, C. Bisagni
Probability-Based Methodology for Buckling Investigation of Sandwich Composite Shells with and Without Cut-Outs
International Journal for Computational Methods in Engineering Science and Mechanics, Vol. 18, N. 1, 2017, p. 77-90
doi:10.1080/15502287.2016.1276353

Probability-based methodology for buckling investigation of sandwich composite shells with and without cut-outs

M. Alfano and C. Bisagni*

Department of Aerospace Science and Technology, Politecnico di Milano, Via La Masa 34, 20156, Milano, Italy

michela.alfano@polimi.i

chiara.bisagni@polimi.it

Currently at Delft University of Technology, Faculty of Aerospace Engineering, Kluyverweg 1, 2629 HS Delft, the Netherlands, C.Bisagni@tudelft.nl.

The objective of the running EU project DESICOS (New Robust DESign Guideline for Imperfection Sensitive COmposite Launcher Structures) is to formulate an improved shell design methodology in order to meet the demand of aerospace industry for lighter structures. Within the project, this paper discusses the development of a probability-based methodology developed at Politecnico di Milano. It is based on the combination of the Stress-Strength Interference Method and the Latin Hypercube Method with the aim to predict the bucking response of three sandwich composite cylindrical shells, assuming a loading condition of pure compression. The three shells are made of the same material, but have different stacking sequence and geometric dimensions. One of them presents three circular cut-outs. Different types of input imperfections, treated as random

variables, are taken into account independently and in combination: variability in longitudinal Young's modulus, ply misalignment, geometric imperfections and boundary imperfections. The methodology enables a first assessment of the structural reliability of the shells through the calculation of a probabilistic buckling factor for a specified level of probability. The factor depends highly on the reliability level, on the number of adopted samples and on the assumptions made in modeling the input imperfections. The main advantage of the developed procedure is the versatility as it can be applied to the buckling analysis of laminated composite shells and sandwich composite shells including different types of imperfections.

Keywords

Probabilistic Methods; Buckling; Probabilistic Buckling Factor; Sandwich Composite Shell; Cut-outs.

ACCEPTED MANUSCRIPT

1. Introduction

Due to their high performance and low weight, sandwich structures are widely used in the aerospace industry, especially in the design of space launch vehicles, where the buckling is one of the dimensioning criteria. The current shell design mainly relies on NASA SP-8007 guideline[1], which provides recommendations for isotropic and laminated composite shells, and for sandwich shells whose facesheets are made of isotropic material and the core is elastic. Such a guideline proposes the use of an empirical knockdown factor to account for the manufacturing and in-service imperfections, which are the primary source of the discrepancy between analytical predictions and experimental results[2,3]. However, the use of the empirical knockdown factor may often lead to overly conservative design. Singer et al.[2] pointed out the availability of imperfection data as one of the prerequisites for developing and validating an advanced shell design methodology. Bisagni[3,4,5] carried out numerical and experimental studies of buckling and post-buckling phenomena of shells and obtained a good numerical-experimental correlation by including the imperfections measured on test specimens into the numerical model. The numerical and experimental investigation of composite cylindrical shells under a loading condition of pure compression and of compression combined with torque displayed the influence of the stacking sequence on the buckling response and the independence of the buckling load on the sequence of application of the two types of load.

In the past twenty years, the literature concerning buckling investigation of axially compressed cylindrical shells has extensively focused on the use of methods of probabilistic analysis with the goal to define stability design methodology[6-9] for shells. Considering the input imperfections in a

probabilistic manner, as proposed by Bolotin[6], allows for assessing the response variability of cylindrical structures. Elishakoff et al.[7] adopted the First-Order Second-Moment Method to predict the structural reliability function of isotropic cylindrical shells and the Monte Carlo Method to verify the results. Through exploiting the two stated approaches, Arbocz and Hilburger[8] developed a probability-based analysis method and applied it to the buckling study of laminated composite shells under pure compression. The goal was to achieve an "improved" knockdown factor starting from input probabilistic parameters that were experimentally derived. The Monte Carlo Method was used by Kriegesmann et al.[9] to perform a probabilistic analysis of laminated composite shells including both geometric and boundary imperfections regarded as random parameters, which were defined on the basis of the results of statistical analysis of experimental measurements. Takano[10] carried out a statistical analysis of buckling test data concerning shells with different geometric dimensions, material and layup from open literature in order to calculate two statistical knockdown factors, the A-basis equal to 0.479 and B-basis equal to 0.626. The main assumption of the statistical analysis of Takano is that the calculated factors are independent on radius over thickness ratio of shells.

The running EU project DESICOS[11] (New Robust DESign Guideline for Imperfection Sensitive COmposite Launcher Structures) has the goal to meet the demand of aerospace industry for lighter structures through the development and the validation of improved shell design criteria. The project is mainly focused on the combination of probabilistic and deterministic approaches including, in particular, the Single Perturbation Load Approach. The Single Perturbation Load Approach was studied by NASA and by Hühne et al.[12] starting from the experimental observation that the dimple shape imperfection is similar to the dimple that forms in a

compressed cylindrical shell at the onset of buckling. The buckling is trigged by a lateral load imposed to the shell before applying the axial compression. By increasing the lateral load, the buckling load decreases up to an almost constant magnitude which is taken as the design load. Orifici and Bisagni[13] studied two laminated composite shells and two sandwich composite shells with a rectangular cut-out by the Single Perturbation Load Approach. Castro et al.[14] made a comparison among different approaches of modeling the geometric imperfections. To this purpose, the buckling load of composite shells, considering different models of imperfections, was graphed as knockdown factor in function of the imperfection amplitude. The results indicated that the axisymmetric geometric pattern seemed to be the most detrimental.

This paper discusses the development of a probability-based methodology, which provides a unified framework for the probabilistic buckling analysis of shells subjected to axial compression. The Stress-Strength Interference Method and the Latin Hypercube Method are combined to perform the probabilistic structural analysis of the scaled models of the Dual Launch System (SYLDA) and of the Interstage Skirt Structure (ISS) of Ariane 5 launcher. The SYLDA model is also studied with the presence of three circular cut-outs (SYLDA with cut-outs). The scaled models of the three shells were designed by Airbus Defence & Space. These structures are three sandwich composite shells made of the same material but with different stacking sequence and geometric dimensions.

The procedure of the probability-based methodology is described, showing the potentiality of a probabilistic analysis. The probabilistic approach aims to assess the probabilistic buckling factor

of the shells taking different types of input imperfections into account, and assuming loading condition of pure compression.

The main advantage of the probability-based methodology is the versatility because it can be applied to buckling analysis of laminated composite shells and sandwich composite shells including different kinds of imperfections and using different sampling techniques. The modeling of input imperfections can be adapted on the basis of the available data and it does not require approximations, against other probabilistic methods like the First-Order Second-Moment Method.

Firstly, the main results of the buckling and post-buckling deterministic analysis of these sandwich shells are presented. Next, the probabilistic buckling analysis is performed using the developed probabilistic procedure.

2. Shells Description and Finite Element Models

The scaled models of the Dual Launch System (SYLDA) and of the Interstage Skirt Structure (ISS) are here investigated. The diameter of the shells is equal to 700 *mm*; the length of SYLDA is equal to 700 *mm*, while the length of ISS is 358 *mm*. As two tabs are bonded to the ends of the shells to perform the experimental tests, the free length is limited to the central part and measures 620 *mm* for SYLDA and 318 *mm* for ISS. A third shell is moreover studied: SYLDA scaled model including the presence of three cutouts. The configuration of SYLDA with cut-outs consists of a cut-out of diameter equal to 92 *mm* located on one side of the shell and two smaller

cut-outs of diameter equal to 46 *mm* on the other side. The centers of the two smaller cut-outs have a distance of 92 *mm*.

The shells are made by a sandwich consisting of two composite facesheets and a core. The facesheets are laminates made of Hexcel IM7/8552 UD carbon prepreg, whose material properties are taken from literature[15,16,17] and are listed in Table 1, with ply thickness of 0.131 *mm*.

The core material is EVONIK Rohacell WF200[18] with thickness of 1.5 *mm* for SYLDA models, and 2.6 *mm* for ISS model. The material properties are reported in Table 2.

The stacking sequence of SYLDA and SYLDA with cut-outs is [19°/-19°/90°/CORE/90°/-19°/19°] for a total thickness equal to 2.286 *mm*, whereas ISS has layup [30°/-30°/0°/CORE/0°/-30°/30°] for a total thickness equal to 3.386 *mm*.

The finite element model of each shell is set up using the commercial FE code ABAQUS 6.13[19] with S4R shell elements. The mesh size of SYLDA and of ISS is equal to 10 *mm* x 10 *mm* and 10 *mm* x 9.94 *mm*, respectively. The finite element model of SYLDA with cut-outs is generated using a global mesh size of 10 *mm* x 10 *mm*. The area around each cut-out is meshed with smaller elements: 4 *mm* x 4 *mm* around the larger cut-out, and 3.6 *mm* x 3.6 *mm* around the two smaller cut-outs.

The shell models are fixed at one edge, while all degrees of freedom except the axial translation are constrained at the loaded edge.

3. Deterministic Buckling and Post-Buckling Analysis

The buckling and post-buckling response of SYLDA, SYLDA with cut-outs and ISS under compression load is analyzed by performing explicit dynamic analysis. The load is introduced through an axial displacement imposed at a loading ratio of 1 *mm/s*. Firstly, nominally perfect geometry is assumed; next, the sensitivity of the shells to axisymmetric geometric imperfections is numerically assessed.

The meshes of SYLDA, SYLDA with cut-outs and ISS are illustrated in Figure 1, where the meshes around the cut-outs are also displayed. The amplified imperfection shape of each shell is shown in the figure.

The imperfection amplitude is quantified by the amplitude to thickness ratio ξ taking into account the total thickness of the shell. Three levels of ξ are here considered: 0%, 10% and 50%.

Figure 2 illustrates the load-shortening curves of SYLDA for the three values of ξ. The NASA knockdown factor[1] is also highlighted in the figure. It is determined using the formulae provided by NASA guideline for laminated composite shells under the assumption that SYLDA is considered as a laminate of seven plies. The nominal response of the shell is linear until buckling which takes place at 1.78 *mm* for a load of 417 *kN*. As the imperfection amplitude increases, the load-carrying capacity of the shell decreases. For ξ equal to 50%, the buckling phenomenon yields a reduction of shell stiffness.

The deformed configurations of SYLDA corresponding to the three levels of ξ are shown in Figure 3 at 2.50 *mm* of shortening. In the case of nominally perfect geometry, the displacement

contour exhibits two rows of buckles along the axial direction. The deformed configuration for ξ equal to 10% is characterized by two rows of fully developed buckles, whereas it displays a chessboard-like pattern for ξ equal to 50%.

The buckling and post-buckling response of SYLDA with cut-outs is predicted for the three levels of ξ and is shown in Figure 4. The geometrically perfect shell presents an initial local instability close to the cut-outs at 0.90 *mm* for a load of 200 *kN*. The shell withstands an additional amount of load until 1.31 *mm* where it buckles globally for 287 *kN*. The collapse occurs at 1.45 *mm* for a load of 294 *kN*. As the imperfection amplitude increases, the maximum load decreases and the response curve changes remarkably.

Figure 5 illustrates the deformed configurations of SYLDA with cut-outs for the three magnitudes of ξ at 2.50 *mm* of imposed shortening. It is possible to note that the cut-outs dominate the buckling response.

Figure 6 reports the load-shortening curves of ISS for the three levels of ξ and the NASA knockdown factor, which is assessed with the assumption that the shell is regarded as a laminate of seven plies.

The shell exhibits a pre-buckling nominal response that is linear up to about 1 *mm* of shortening; later, the slope of the load-shortening curve decreases, indicating a non-linear behavior. At 1.23 *mm* and 513 *kN* the load drops and an instability phenomenon develops. As the imperfection amplitude ξ increases, ISS displays a gradual reduction of pre-buckling stiffness. The sudden drop of load following the buckling is observed only for the nominally perfect structure.

The deformed configurations of ISS are illustrated in Figure 7. The post-buckling pattern of the shell without imperfections presents a single row of buckles, while the shell with imperfections shows axisymmetric deformation.

4. Probabilistic Procedure for Buckling Analysis

Figure 8 illustrates the block diagram of the probability-based methodology, which is developed by combining the Stress-Strength Interference Method and the Latin Hypercube Method in order to perform a probabilistic structural analysis for axially compressed cylindrical shells. The goal is to determine the probabilistic buckling factor for a probability level equal to 99%.
This factor enables to evaluate the sensitivity of the shell to the different types of input imperfections, but is highly influenced by the assumed variability of the input parameters, by the adopted sample size and by the required standard of probability. The influence of the input imperfections, treated in probabilistic manner, is assessed separately and in combination. The imperfections here considered are geometric imperfections, non-uniform loading effects and variability in longitudinal Young's modulus and in laminae orientation. The product between the probabilistic buckling factor and the buckling load of the nominally perfect shell is the load associated with 99% probability that the shell withstands compression load without undergoing buckling.

4.1. Probabilistic Properties of Imperfection Parameters

The parameters of the different kinds of input imperfections considered in the probabilistic analysis are here described.

4.1.1. Geometric Imperfections

The geometric imperfections are defined as the radial deviation of the effective surface of the shell from the nominal one. The geometric imperfections applied to the nominal geometry of each shell are the same used in the deterministic investigation and shown in Figure 1. They are assumed to have an axisymmetric shape modeled by the sine function $w/t = \xi \sin(i\pi z/l)$ where *w* is the radial displacement, *t* and *l* are the total thickness and the length of the shell, and *z* is the axial direction. The number of axial half-waves *i* is selected equal to 12 for SYLDA and SYLDA with cut-outs because a numerical investigation has shown that this shape results to have the most detrimental effect on the load-carrying capability of the shells. The axisymmetric imperfections have been selected also for ISS and in this case the number of axial half-waves *i* is set to 4, equal to the first buckling mode. The imperfection amplitude ξ is here assumed to be a random variable.

Arbocz and Hilburger[8] described the geometric imperfections using a two-mode initial imperfection model, whose parameters were determined from experimental measurements of laminated composite shells. The mean value $\bar{\xi}$ and the standard deviation s_ξ of the imperfection amplitude are here taken on the basis of Ref. 8 considering the worst case of superposition of the two reported modes: $\xi \sim N(\bar{\xi}, s_\xi) = N(-0.0083, 0.0316)$..

4.1.2. Variability in Longitudinal Young's Modulus

An experimental program to identify the statistical properties of the Hexcel IM7/8552 UD Carbon Prepreg is described in literature[20]. The mean value and standard deviation of the longitudinal Young's modulus E_{11} are equal to 171.42 *GPa* and 2.38 *GPa*, respectively. These

statistical estimators are referred to the tensile properties of the material. Since statistic data of the compression properties of the material are not available, the ones of tensile properties are here used in order to illustrate the probabilistic procedure.

Current practices[21] recommend the use of material design allowables to reduce the probability of material failure due to material properties variability, manufacturing process variations, etc. They are material property values that are statistically calculated from test data. Typical allowable design values are the A-basis and B-basis. The A-basis is the allowable value that is exceed by 99% of population of the material property with 95% confidence level to be exceed. The B-basis is the allowable value that is exceed by 90% of population of the material property with 95% confidence level to be exceed.

On the hypothesis that the longitudinal Young's modulus is normally distributed with $E_{11} \sim N\left(\overline{E}_{11}, s_{E_{11}}\right) = N(171.42\ GPa, 2.38\ GPa)$,, the B-basis and A-basis allowable design values of E_{11} are equal to 163 *GPa* and 158 *GPa*. The material design allowable that is exceed by 99.99% of population of E_{11} with 95% confidence level to be exceed is equal to 150 *GPa*. It is identical to the compressive longitudinal Young's modulus reported in Refs. 15, 16, 17 and in Table 1 and used in the deterministic buckling analysis of the three shells. Since the variability of the longitudinal Young's modulus is here treated in a probabilistic manner, the adopted mean value of E_{11} is equal to 171.42 *GPa* and not 150 *GPa*.

A preliminary probabilistic investigation of the three shells with variability of E_{11} displayed that the assumption of $E_{11} \sim N(171.42\ GPa, 2.38\ GPa)$ yields results less conservative than the ones obtained by deterministic buckling analysis using material design allowable equal to 150 *GPa*. In

order to be conservative, the upper bound of the 95% confidence interval of the standard deviation $s_{E_{11}}$ of E_{11} is used in place of $s_{E_{11}}$. The probabilistic study of the influence of the longitudinal Young's modulus is so carried out under the assumption that $E_{11} \sim N(171.42\ \text{GPa}, 6.84\ \text{GPa})$. The value of E_{11} is regarded identical for each lamina, because it is supposed that all laminae come from the same batch of production.

4.1.3. Ply Misalignment

The orientation of each lamina is taken to have a Gaussian distribution with mean value equal to the nominal value of the angle and a tolerance of ±2°, typical in the aerospace industry. The angles are regarded independent on each other. As consequence of the assumption of independence, the laminate resulting from the application of the Latin Hypercube Method can present anisotropy.

4.1.4. Boundary Imperfections

The boundary imperfections are modeled as deviations from the uniform distribution of axial displacement imposed along the loaded edge. They are simulated using a one-dimensional homogeneous Gaussian field (i.e., a random function of the circumferential coordinate), whose mean value is equal to the nominal magnitude of applied axial displacement and the covariance Σ is modeled by the exponential function[22] $\Sigma=\Sigma_0 \exp(-|d|/l_0)$, where d is the circumferential distance between two nodes of the loaded edge, l_0 is the correlation length set to πr and r is the radius of the shell. The variance Σ_0 of the Gaussian field is taken so that the resulting profile of the reaction forces has a coefficient of variation equal to 15%. The coefficient of variation is the ratio between the standard deviation and the absolute value of the mean. Σ_0 is set on the basis of

Ref. 23 where it is reported a coefficient of variation associated to the launch vehicle static loads due to the thrust equal to 5%. As the shell is also subjected to other static loads during the launch, this value is tripled to be conservative.

4.2. Stress-Strength Interference Method and Limit-State Function

One of the most widely used method for the structural reliability analysis is the Stress-Strength Interference Method[24,25]. The overlap region of the probabilistic distributions of limit stress and stress of the structure determines the conditions under which it does not fail, that is the structural reliability R_e. The difference between limit stress and stress is the limit-state function $g(X)$. In buckling analysis of axially compressed cylindrical shells, the limit-state function $g(X)$ can be constructed as the difference between the normalized buckling load Λ_s of the structure and the normalized loading parameter, named here probabilistic buckling factor λ: $g(X) = \Lambda_s(X)-\lambda$. The vector X includes the input random variables. The normalized buckling load $\Lambda_s(X)$ is considered a random variable: it is characterized through its probability distribution function caused by the variability of the input imperfections. The normalization is performed with respect to the critical load of the shell without any imperfections.

The probabilistic buckling factor λ is a constant random variable (i.e., it takes a single constant value with unitary probability) and has to be determined on the basis of the sources of imperfections. It is assessed by the definition of the reliability function $R_e(\lambda)$, which is the probability that the limit-state function is positive:

$$R_e(\lambda) = \text{Prob}(g(X) > 0) = \text{Prob}\left(\Lambda_s(X) > \lambda\right) = \int_{\lambda}^{\infty} f_{\Lambda_s}(\Lambda_s)\, d\Lambda_s = 1 - F_{\Lambda_s}(\lambda) \quad (4.1)$$

where $f_{\Lambda_s}(\Lambda_s)$ and $F_{\Lambda_s}(\Lambda_s)$ are the probability density function and the cumulative density function of $\Lambda_s(X)$, respectively. They are unknowns and are determined using the Latin Hypercube Method. The reliability is therefore defined as the probability that the shell does not buckle under compression load.

Thus, once the requirement of reliability level is specified and the probability distribution function of $\Lambda_s(X)$ is identified, the corresponding λ is assessed by Eq. (4.1).

4.3. Latin Hypercube Method and Distribution Identification

The Latin Hypercube Method[22] is applied in order to generate a data collection of the buckling load given the input imperfections. The general procedure of the Latin Hypercube Method is illustrated in Figure 8. It differs from the Monte Carlo Method[25,26] because the Monte Carlo Method draws samples from uniform distribution, whereas the Latin Hypercube Method uses the Latin Hypercube Sampling, reducing so the variance of probabilistic buckling factor estimated by the probabilistic methodology. This sampling method is a form of stratified sampling where the marginal distribution of each variable is divided into *N* intervals of equal probability and then a value is selected from each of the intervals. The *N* samples generated by the Latin Hypercube Sampling cover the range of the distribution in much fewer samples than would be required to cover the range with purely random samples.

A sample size *N* equal to 100 is chosen in this study in order to keep a limited computational time. As a consequence of the low number of random variables included here into the probabilistic analysis, a convergence study has proven that the adopted sample size provides satisfactory precise results. *N* samples of each input random variable are generated through the

Latin Hypercube Sampling and are then incorporated independently or in combination in the finite element model of shell. The simulation of the *N* finite element models of the shell with imperfections is carried out using FE code ABAQUS 6.13. *N* displacement-control implicit dynamic analyses are run at a loading ratio of 1 *mm/s*. Implicit analysis is here preferred to explicit analysis in order to save computational time. The obtained critical loads are then normalized to achieve the data collection of $\Lambda_s(X)$.

The data collection is used to identify the statistical characteristics and the distribution of $\Lambda_s(X)$ by means of goodness-of-fit statistics. They are statistical measurements that enable to reject or accept the assumption that the data have a given distribution. Three techniques, the Probability Plot (e.g., quantile-quantile plot), the Kolmogorov-Smirnov test and the Anderson-Darling test, are here adopted to choose the distribution that best fits the observations of $\Lambda_s(X)$. The histogram and the statistical estimators (mean value, standard deviation, coefficient of variation, skewness, etc.) of tests of $\Lambda_s(X)$ allow to draw few conclusions about the distribution of the normalized buckling load.

The distribution of $\Lambda_s(X)$ is limited in such a way that the probabilistic buckling factor cannot assume values larger than one:

$$F_{\Lambda_s}(\Lambda_s) = \begin{cases} \dfrac{F_{\Lambda_s}(\Lambda_s)}{F_{\Lambda_s}(1)} & \text{if} \quad \Lambda_s < 1 \\ 1 & \text{if} \quad \Lambda_s \geq 1 \end{cases} \qquad f_{\Lambda_s}(\Lambda_s) = \begin{cases} \dfrac{f_{\Lambda_s}(\Lambda_s)}{F_{\Lambda_s}(1)} & \text{if} \quad \Lambda_s < 1 \\ 0 & \text{if} \quad \Lambda_s \geq 1 \end{cases} \tag{4.2}$$

$F_{\Lambda_s}(1)$ stands for the cumulative density function of $\Lambda_s(X)$ that is evaluated in $\Lambda_s(X) = 1$.

4.4. Assessment of Probabilistic Buckling Factor

After having defined the distribution of the normalized buckling load, the probabilistic buckling factor λ is estimated through Eq. (4.1), using the inverse cumulative density function $F_{\Lambda_s}^{-1}$ of $\Lambda_s(X)$, for a probability level of 99%:

$$R_e = \text{Prob}\left(\Lambda_s(X) > \lambda \right) = 1 - F_{\Lambda_s}(\lambda) \quad \overset{\text{yields}}{\rightarrow} \quad \lambda = F_{\Lambda_s}^{-1}\left(1 - R_e \right) \qquad (4.3)$$

This factor corresponds to the load value such that the probability that the shell withstands compression load without undergoing buckling is equal to 99%. In the case that the normalized buckling load is normally distributed and is uncorrelated from the probabilistic buckling factor, Eq. (4.3) can be re-formulated using the reliability index $\beta = (\overline{\Lambda}_s - \lambda)/s_{\Lambda_s}$ and the relationship $R_e = \Phi(\beta)$[22]:

$$R_e = \Phi(\beta) = \Phi\left(\frac{\overline{\Lambda}_s - \lambda}{s_{\Lambda_s}} \right) \overset{yields}{\longrightarrow} \lambda = \overline{\Lambda}_s - \beta \cdot s_{\Lambda_s} \qquad (4.4)$$

where Φ is the standard normal cumulative density function. The probabilistic buckling factor is thus expressed as a function of the sample mean value $\overline{\Lambda}_s$, the sample standard deviation s_{Λ_s} of $\Lambda_s(X)$ and of the reliability index β. This is the margin between the mean value of $\Lambda_s(X)$ and the loading parameter λ normalized by the standard deviation of $\Lambda_s(X)$. A reliability of 99% implies a reliability index of 2.33.

The use of Eq. (4.3) rather than of Eq. (4.4) relies on which probabilistic distribution, Gaussian or not Gaussian, is identified to best describe the buckling response $\Lambda_s(X)$ of shell.

5. Results

The developed probabilistic procedure for buckling analysis is here applied to the study of SYLDA, SYLDA with cut-outs and ISS, assuming loading conditions of pure compression. The probabilistic buckling factor is calculated to define the sensitivity of the three shells to the input imperfections, whose influence is investigated independently and in combination.

5.1. Probabilistic Buckling Analysis of SYLDA Shell

Table 3 summarizes the results of the probabilistic buckling analysis of the scaled model of SYLDA. The probabilistic buckling factor λ of the shell is estimated for a probability level equal to 99% in the different analysis cases.

To obtain the data collection $\Lambda_s(X)$, the data set of buckling load is normalized by the buckling load of the nominally perfect shell, which is equal to 459 *kN*. The nominally perfect shell refers to the scaled model of SYLDA considering the nominal values of the input imperfections. It corresponds to SYLDA without geometric and boundary imperfections, without error of ply angles and with longitudinal Young's modulus E_{11} of laminae equal to 171.42 *GPa*. Indeed, the influence of the variability in material properties is here studied in probabilistic manner rather than taken into account through the allowables.

The NASA knockdown factor is determined for SYLDA using the formulae recommended in NASA SP-8007 guideline[1] for laminated composite shells on the hypothesis that SYLDA can be considered a laminate of seven plies. It is equal to 0.57 and corresponds to a load of 262 *kN*.

Table 3 points out that, among all imperfections, the geometric imperfections turn out to be the most dominant in determining the buckling response of SYLDA. When the boundary imperfections, the variability of longitudinal Young's modulus and the ply misalignment are considered in addition to the geometric imperfections, the λ value of the shell decreases from 0.73 to 0.71. However, the individual influence of the boundary imperfections drops the buckling load of SYLDA by 11%.

The three goodness-of-fit tests are used to verify the assumption that the normalized buckling load $\Lambda_s(X)$ of SYLDA shell combining all the sources of input imperfections is normally distributed.

The quantile-quantile plot of Gaussian distribution is shown in Figure 9. The black line stands for the Gaussian quantile $Q_N(q)$ that is expressed as a linear function of the standard Gaussian quantile $Q_1(q)$:

$$Q_N(q) = F^{-1}_{\Lambda_s}(q) = \overline{\Lambda}_s + s_{\Lambda_s}\Phi^{-1}(q) = \overline{\Lambda}_s + s_{\Lambda_s}Q_1(q) \qquad (5.1)$$

where q is the empirical cumulative density function; $\overline{\Lambda}_s$ and s_{Λ_s} are the sampled mean value and the sampled standard deviation of the tests of $\Lambda_s(X)$, respectively. The dotted gray lines in the figure represent the 95% confidence bounds of the quantile $Q_N(q)$. Since the data collection of $\Lambda_s(X)$, depicted as empty circles on the Gaussian quantile-quantile plot in the figure, falls approximately on a straight line and no data are outside the confidence interval, the data set follows the Gaussian distribution.

The Kolmogorov--Smirnov statistic quantifies the distance between the empirical and the Gaussian cumulative density functions. The two distributions are compared in Figure 10. The maximum percentage distance between them is equal to 5%. The empirical cumulative density function presents a swinging trend due to the use of a sample of the population of $\Lambda_s(X)$.

The procedure of the Anderson-Darling (AD) test is applied to the observations of $\Lambda_s(X)$. The *AD* test statistic is calculated in accordance with Ref. 21:

$$AD = -N - \sum_{i=1}^{N} \frac{2i-1}{N} \left[\ln F_{\Lambda_s}\left(\Lambda_{s,\,i}\right) - \ln\left(1 - F_{\Lambda_s}\left(\Lambda_{s,\,N+1-i}\right)\right)\right] = 0.30 \tag{5.2}$$

and the modified Anderson-Darling test is obtained as $AD^{*}=AD\left(1+0.2/\sqrt{N}\right)=0.30$.

The decision to reject or not to reject the assumption that data have the hypothesized distribution is based on the comparison between the observed significance level *OSL* and the recommended significance level α of the test. The *OSL* for the Gaussian distribution is:

$$OSL = \frac{1}{1 + \exp\left(-0.48 + 0.78\ln\left(AD^{*}\right) + 4.58\, AD^{*}\right)} = 0.51 \tag{5.3}$$

Since $OSL > \alpha = 0.05$, the assumption of Gaussian distribution is not rejected. The significance level is here set to 0.05, because the value $1-\alpha = 95\%$ is by far the most commonly used confidence level.

As consequence of the results of the three goodness-of-fit tests, the normalized buckling load $\Lambda_s(X)$ of SYLDA shell with joint imperfections is accepted to have a Gaussian distribution.

In the assumption that $\Lambda_s(X)$ is normally distributed, the reliability $R_e(\lambda)$ of SYLDA including the input random variables in combination is determined by Eq. (4.4) as function of the probabilistic buckling factor λ and plotted in Figure 11.

The region below the curve represents the "safe region" where the shell withstands axial load without undergoing buckling; on the contrary, the buckling takes place in the "unsafe region" above the curve. The dashed black line highlights the λ value of the shell, equal to 0.71, for 99% probability. The corresponding value of buckling load of SYLDA combining all the sources of imperfections is equal to 326 *kN*. This outcome depends highly on the modeling of the input random variables. For instance, changing the shape and the amplitude of the geometric imperfections, the resulting λ differs. As an example, the probabilistic buckling factor falls off by 26% with a tripling of the standard deviation of the imperfection amplitude. Increasing the requirement of probability, the resulting λ decreases, as evident in Figure 11. For instance, the probabilistic buckling factor drops from 0.71 to 0.61 when the reliability level is raised from 99% to 99.99%.

The evaluated probabilistic buckling factors is affected by the sample size. As an example, the convergence study reveals that the λ factor of SYLDA with joint imperfections turns out to be 0.70 for a number of simulations equal to 300. Hence, in this case, the adopted sample size of 100 provides satisfactory precise results.

The deterministic buckling analysis of SYLDA was performed using longitudinal Young's modulus E_{11} equal to 150 *GPa*. The reduction of E_{11} from the mean value 171.42 *GPa* to the design allowable 150 *GPa* decreases the buckling load of SYLDA from 459 *kN* to 417 *kN*. The

superposition of the axisymmetric geometric imperfections for ξ = 10% causes an additional reduction of the buckling load from 417 *kN* to 304 *kN* as shown in Figure 2. On the other side, the load corresponding to the λ factor which is obtained by the probabilistic analysis of SYLDA combining all input probabilistic parameters is equal to 326 *kN*. Consequently, the buckling load assessed by the developed probabilistic procedure is 7% higher than the deterministic one obtained with design allowable Young's modulus and geometric imperfections with amplitude equal to 10% of the thickness.

5.2. Probabilistic Buckling Analysis of SYLDA Shell with Cut-outs

The probabilistic methodology is applied to the buckling analysis of SYLDA with cut-outs in order to realize a data collection of $\Lambda_s(X)$. The normalized buckling load is, in particular, obtained from the division of the maximum load reached by the shell with imperfections by the maximum load reached by the nominally perfect shell, which is equal to 325 *kN*. The maximum load is considered rather than the local buckling load because the load-carrying capacity of the structure is here of interest.

Table 4 lists the probabilistic buckling factor λ of SYLDA with cut-outs which is evaluated in the different analysis cases for a probability of 99%. The knockdown factor is not available for this shell because NASA monographs do not provide recommendations for cylindrical shells with cut-outs.

From Table 4 it is possible to note that for SYLDA with cut-outs the λ value is not dominated by a specific source of imperfections, but is the result of the joint influence of all input parameters.

The load-shortening curve of SYLDA with cut-outs and without including imperfections is shown in the left graph of Figure 12. The dotted black line represents the maximum load of 325 *kN* reached by the nominally perfect shell. In the right graph of Figure 12 the probability density function $f_{\Lambda_s}(\Lambda_s)$ of the normalized buckling load of SYLDA with cut-outs and combining all the input imperfections is illustrated. The dotted black line stands for the unitary normalized buckling load. The probabilistic buckling factor λ equal to 0.87, obtained for a probability of 99%, is highlighted on the distribution $f_{\Lambda_s}(\Lambda_s)$. The Figure 12 shows also that λ value for 99% probability corresponds to a maximum load of SYLDA with cut-outs and imperfections equal to 283 *kN*.

Few conclusions can be drawn from the right graph of Figure 12. Firstly, the dispersion of $\Lambda_s(X)$ caused by input probabilistic variables is low: the mean value and the coefficient of variation of $\Lambda_s(X)$ are equal to 0.97 and 4%, respectively. It is likely due to the presence of the cut-outs whose effect prevails in determining the buckling response. The consequence of the truncation is here remarkable, because few samples of $\Lambda_s(X)$ are higher than the unity. This outcome is mainly attributable to the boundary imperfections. If the profile of axial displacement generated by the Latin Hypercube Sampling has the lowest magnitude in the circumferential portion of loaded edge that coincides with the location of the cut-outs, the shell reaches a maximum load higher than the nominal one.

A simulation obtained by the Latin Hypercube Method for the probabilistic analysis of the shell with boundary imperfections is here illustrated.

Figure 13 reports the sampled boundary imperfections. A planar view, representing the unfolded shell, is provided in the top of the figure. The circumferential portion of the edge which

coincides with the position of the isolated cut-out is the least loaded. The consequence is that the shell reaches a higher load before the snap-through as shown in Figure 14. The maximum load is equal to 331 *kN* for 1.44 *mm* of shortening.

Figure 15 illustrates the radial displacement contour of the shell corresponding to the three points reported on the load-shortening curve. The boundary imperfections do not modify the deformed configuration of the shell.

The deterministic buckling analysis of SYLDA with cut-outs was carried out using longitudinal Young's modulus equal to 150 *GPa*. The reduction of E_{11} from the mean value 171.42 *GPa* to the design allowable 150 *GPa* decreases the maximum load reached by SYLDA with cut-outs from 325 *kN* to 294 *kN*. When the axisymmetric geometric imperfections are superposed for ξ equal to 10% to the nominal geometry of the shell, the maximum load decreases from 294 *kN* to 259 *kN*. By the probabilistic analysis, the load corresponding to the λ factor of SYLDA with cut-outs and joint imperfections is 283 *kN*. The probabilistic maximum load is 9% higher than the deterministic one.

5.3. Probabilistic Buckling Analysis of ISS Shell

Table 5 summarizes the probabilistic buckling factor λ of ISS shell which is assessed for a requirement of probability equal to 99%. To obtain the data collection $\Lambda_s(X)$, the data set of buckling load is normalized by the buckling load of the nominally perfect shell, which is equal to 545 *kN*.

The NASA knockdown factor of ISS is equal to 0.64. The corresponding load value is equal to 349 *kN*. Such a factor is determined under the assumption that ISS can be considered as a laminated composite shell of seven plies in accordance with NASA monographs[1].

Table 5 shows that the shell is more sensitive to the geometric imperfections than to other types of imperfections. The variability of the longitudinal Young's modulus and the ply misalignment do not affect significantly the buckling load of the shell. The low sensitivity to an error of ply angles depends on the short length of the shell. The boundary imperfections cause a reduction of 8%, whereas the individual influence of the geometric imperfections decreases the critical load by 16%. The buckling load of ISS considering the imperfections in combination is equal to 431 *kN*.

The histogram and the empirical probability density function of the observations of $\Lambda_s(X)$ of ISS with combined input imperfections are shown in Figure 16. These two graphical representations are an estimate of the true probability density function of $\Lambda_s(X)$. Few tests of $\Lambda_s(X)$ present values greater than one: these cases correspond to the simulations in which the drawn sample of longitudinal Young's modulus is higher than the nominal one, the drawn sample of imperfection amplitude is close to zero, the drawn samples of ply angle are close to zero (axial direction) and the variation of the imposed axial displacement is low. Besides, the empirical probability density function does not display a pronounced peak. It follows that a larger sample size would be needed to define if this outcome is due to lack of data or if it is an inherent characteristic of the shell response.

The truncated Weibull distribution, which is verified to best fit the data collection of $\Lambda_s(X)$, is also shown in Figure 16. The limitation of the Weibull distribution generates a truncated distribution that captures the location of the peak, but not its frequency. The left tail is besides larger than the one of the empirical distribution. The probabilistic buckling factor is also

displayed in the figure along with the NASA knockdown factor in order to show its position with respect to the data collection of $\Lambda_s(X)$.

6. Comparison of Probabilistic Buckling Factors with NASA knockdown factors

Table 6 lists the NASA knockdown factor[1] estimated for the scaled models of SYLDA and ISS. The probabilistic buckling factors λ of SYLDA, SYLDA with cut-outs and ISS evaluated with the presented methodology are also reported. They are obtained in the analysis cases that consider the input imperfections in combination for a probability of 99%. The resulting λ values of the scaled models of SYLDA and of ISS are mainly caused by the influence of the axisymmetric geometric imperfections, whereas the scaled model of SYLDA with cut-outs is less imperfection sensitive since the cut-outs dominate the buckling response.

The probabilistic buckling factor, which is assessed by the developed probabilistic approach, does not cover the factor of safety that is commonly used for the dimensioning and the design verification of structures.

The probabilistic buckling factors determined by the discussed methodology are based on a random sample of population. This sample consists of a collection of N values of buckling load that are numerically generated. The variability of the results due to the sample constraint needs to be quantified by constructing statistical intervals around the estimated λ value. The probabilistic buckling factors depend also on the specified level of probability and on the modeling adopted for the input random variables.

7. Conclusions

A probability-based methodology for a first assessment of the structural reliability of cylindrical shells is developed by combining two reliability analysis methods, the Strength-Stress Interference Method and the Latin Hypercube Method. The methodology aims to be a unified framework for the probabilistic buckling analysis of axially compressed shells. The goal is to determine the probabilistic buckling factor for a given probability level that the shell withstands axial compression without undergoing buckling. This factor is a measurement of the sensitivity of the shell to the sources of input imperfections, but is highly affected by the required standard of probability, by the modeling of the input random parameters and by the adopted sample size that is here set to 100 in order to decrease computational time and costs.

The probabilistic methodology is applied to the buckling analysis of three sandwich composite cylindrical shells made of the same materials, but with different stacking sequence and geometric dimensions. One of the shells presents three circular cut-outs. The probabilistic buckling factor, which is assessed for a probability of 99%, defines the sensitivity of the three sandwich shells to four sources of imperfections, whose influence is here evaluated independently and in combination. In particular, geometric imperfections, boundary imperfections, variability of longitudinal Young's modulus and ply misalignment are here investigated.

The discussed procedure entails the advantage to be versatile. It is applicable to the buckling analysis of laminated composite shells and sandwich composite shells, and can be used to predict the buckling load of shells taking into account imperfections of different types. The methodology would be useful in predicting the lower bound buckling load of shell, once a database of

measured imperfections pertinent to the shell of interest is available. The measured data should include all of the relevant imperfections, which greatly affect the buckling response. For instance, imperfections concerning the manufacturing processes, the loading conditions and the boundary conditions should be taken into account. Moreover, the database should be large enough to result in a statistically valid estimate of the probabilistic buckling factor.

Acknowledgments

The research leading to these results has received partially funding from the European Community's Seventh Framework Programme (FP7/2007-2013) under Priority Space, Grant agreement no. 282522 (www.desicos.eu). The information in this paper reflects only the authors views and the European Community is not liable for any use that may be made of the information contained herein.

References

1. NASA SP-8007 - Buckling of thin-walled circular cylinders, National Aeronautics and Space Administration, Washington, DC, USA (1968).

2. J. Singer, H. Abramovich and T. Weller, The prerequisites for an advanced design methodology in shells prone to buckling, in *New Approaches to Structural Mechanics, Shells and Biological Structures*, eds. H. R. Drew and S. Pellegrino (Springer, 2002), pp. 393-411.

3. C. Bisagni, Numerical analysis and experimental correlation of composite shell buckling and post-buckling, *Composites Part B*, **31**(8) (2000) 655-667.

4. C. Bisagni and P. Cordisco, An experimental investigation into the buckling and post-buckling of CFRP shells under combined axial and torsion loading, *Composite Structures*, **60**(4) (2003) 391-402.

5. C. Bisagni, Experimental buckling of thin composite cylinders in compression, *AIAA Journal*, **37**(2) (1999) 276-278.

6. V. V. Bolotin, NASA TT F-85 - Statistical methods in the nonlinear theory of elastic shells, National Aeronautics and Space Administration, Washington, DC, USA (1962).

7. I. Elishakoff, S. Van Manen, P. G. Vermeulen and J. Arbocz, First-order second-moment analysis of the buckling of shells with random imperfections, *AIAA Journal*, **25**(8) (1987) 1113-1117.

8. J. Arbocz and M. W. Hilburger, Toward a probabilistic preliminary design criterion for buckling critical composite shells, *AIAA Journal*, **43**(8) (2005) 1823-1827.

9. B. Kriegesmann, R. Rolfes, C. Hühne, J. Teßmer and J. Arbocz, Probabilistic design of axially compressed composite cylinders with geometric and loading imperfections, *International Journal of Structural Stability and Dynamics*, **10**(4) (2010) 623-644.

10. A. Takano, Statistical knockdown factors of buckling anisotropic cylinders under axial compression, *Journal of Applied Mechanics*, **79**(5) (2012) 051004.1-051004.17

11. http://www.desicos.eu/

12. C. Hühne, R. Rolfes, E. Breitbach and J. Teßmer, Robust design of composite cylindrical shells under axial compression – Simulation and validation, *Thin-Walled Structures*, **46**(7-9) (2008) 947-962.

13. A. C. Orifici and C. Bisagni, Perturbation-based imperfection analysis for composite cylindrical shells buckling in compression, *Composite Structures*, **106** (2013) 520-528.

14. S. G. P. Castro, R. Zimmermann, M. A. Arbelo, R. Khakimova, M. W. Hilburger and R. Degenhardt, Geometric imperfections and lower-bound methods used to calculate knock-down factors for axially compressed composite cylindrical shells, *Thin-Walled Structures*, **74** (2014) 118-132.

15. C. Bisagni, R. Vescovini and C. G. Dávila, Single-stringer compression specimen for the assessment of damage tolerance of postbuckled structures, *Journal of Aircraft*, **48**(2) (2011) 495-502.

16. C. Alexandre and P. Blanchard, Definition of the reduced model, ASTRIUM-F (2013).

17. http://www.hexcel.com/Resources/DataSheets/Prepreg-Data-Sheets/8552_eu.pdf.

18. http://www.rohacell.com/sites/dc/Downloadcenter/Evonik/Product/ROHACELL/product-information/ROHACELL%20WF%20Product%20Information.pdf

19. ABAQUS 6.13 Online Documentation, 2013.

20. P. P. Camanho, P. Maimí and C. G. Dávila, Prediction of size effects in notched laminates using continuum damage mechanics, *Composite Science and Technology*, **67** (2007) 2715-2727.

21. MIL-HDBK-17-1F – Composite materials handbook, Department of Defence, USA (2002).

22. **S. K. Choi, R. V. Grandhi and R. A. Canfield,** *Reliability-Based Structural Design* (Springer-Verlag, 2007).

23. T. De Mollerat, C. Vidal and M. Klein, Reliability based factor of safety for unmanned spacecrafts, in *Structural Safety Evaluation Based on System Identification Approaches,* eds. H. G. Natke and J. T. P. Yao (Springer, 1988), pp. 266-312.

24. I. Elishakoff, *Safety Factors and Reliability: Friends or Foes?* (Kluwer Academic Publishers, 2004)

25. C. R. Sundararajan*, Probabilistic Structural Mechanics Handbook, Theory and Industrial Applications* (Chapman & Hall, **1995).**

26. DOT/FAA/AR-99/2 - Probabilistic design methodology for composite aircraft structures, Federal Aviation Administration, USA (1999).

Table 1. Hexcel IM7/8552 UD carbon prepreg.

Property	**Value**
Longitudinal modulus, E_{11}	150000 MPa
Transverse modulus, E_{22}	9080 MPa
Shear modulus, G_{12}	5290 MPa
Poisson's ratio, ν_{12}	0.32
Density, ρ	1570 kg/m^3

Table 2. EVONIK Rohacell WF200.

Property	**Value**
Young modulus of core, E	350 MPa
Shear modulus, G	150 MPa
Poisson's ratio, ν	0.33
Density, ρ	205 kg/m^3

Table 3. Probabilistic buckling factors and corresponding loads of SYLDA.

Analysis case	**Probabilistic buckling factor, λ**	**Load [kN**
Nominal analysis case		459
Probabilistic analysis with geometric imperfections	0.73	335
Probabilistic analysis with variability in longitudinal Young's modulus	0.92	422
Probabilistic analysis with ply misalignment	0.97	445
Probabilistic analysis with boundary imperfections	0.89	409
Probabilistic analysis with combined imperfections	0.71	326

Table 4. Probabilistic buckling factors and corresponding loads of SYLDA with cut-outs.

Analysis case	**Probabilistic buckling factor, λ**	**Load [kN]**
Nominal analysis case		325
Probabilistic analysis with geometric imperfections	0.90	293
Probabilistic analysis with variability in longitudinal Young's modulus	0.93	302
Probabilistic analysis with ply misalignment	0.97	315
Probabilistic analysis with boundary imperfections	0.94	306
Probabilistic analysis with combined imperfections	0.87	283

Table 5. Probabilistic buckling factors and corresponding loads of ISS.

Analysis case	**Probabilistic buckling factor, λ**	**Load [kN]**
Nominal analysis case		545
Probabilistic analysis with geometric imperfections	0.84	456
Probabilistic analysis with variability in longitudinal Young's modulus	0.96	523
Probabilistic analysis with ply misalignment	0.99	540
Probabilistic analysis with boundary imperfections	0.92	501
Probabilistic analysis with combined imperfections	0.79	431

Table 6. NASA knockdown factors and probabilistic buckling factors of the three sandwich shells.

	SYLDA	**SYLDA with cut-outs**	**ISS**
NASA knockdown factor[1]	0.57	N/A	0.64
Probabilistic buckling factor, λ	0.71	0.87	0.79

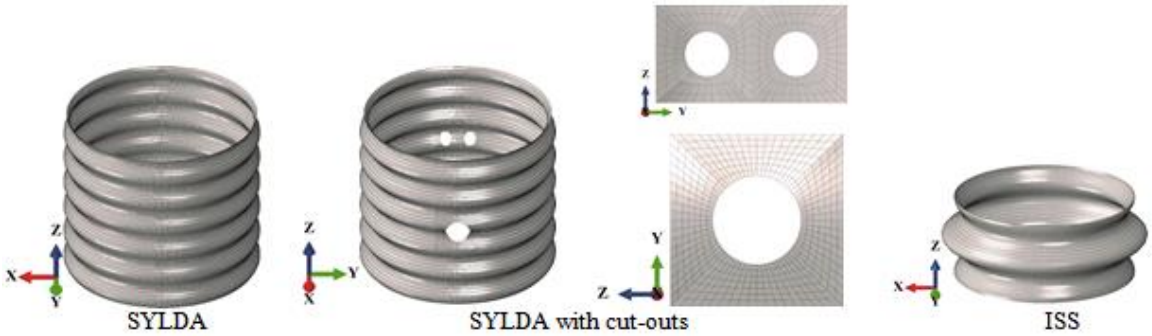

Figure 1. Finite element mesh and amplified geometric imperfection shape of three sandwich shells.

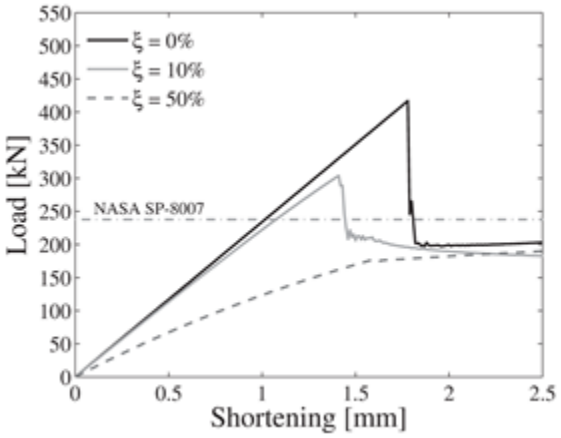

Figure 2. Load-shortening curves of SYLDA with geometric imperfections.

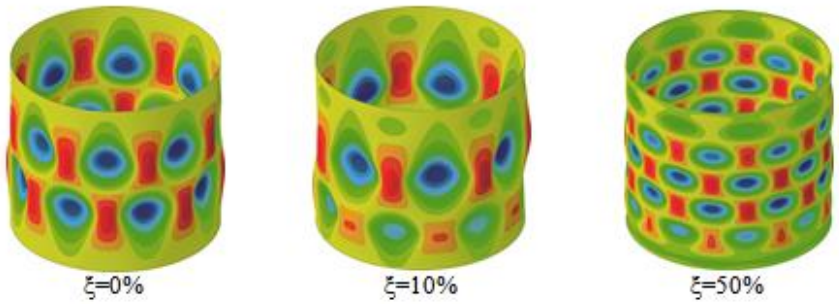

Figure 3. Deformed configurations of SYLDA with geometric imperfections at 2.50 mm.

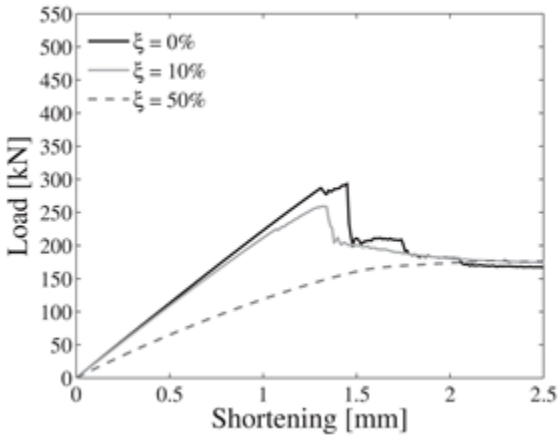

Figure 4. Load-shortening curves of SYLDA with cut-outs and geometric imperfections.

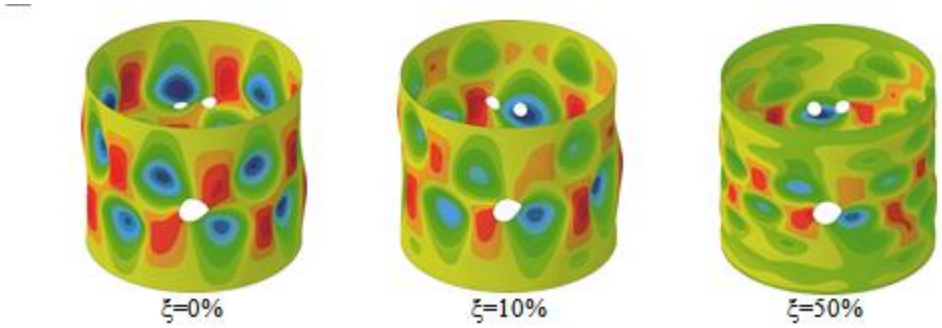

Figure 5. Deformed configurations of SYLDA with cut-outs and geometric imperfections at 2.50 mm.

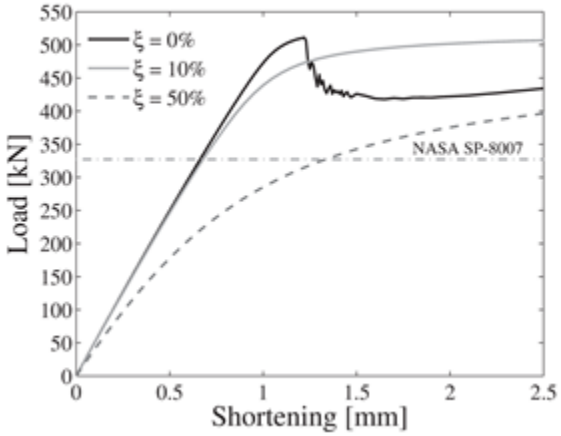

Figure 6. Load-shortening curves of ISS with geometric imperfections.

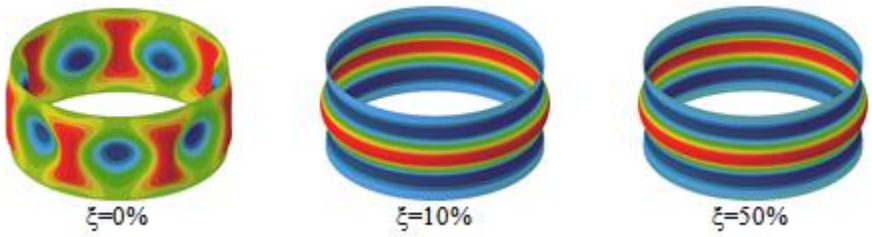

Figure 7. Deformed configurations of ISS with geometric imperfections at 2.50 mm.

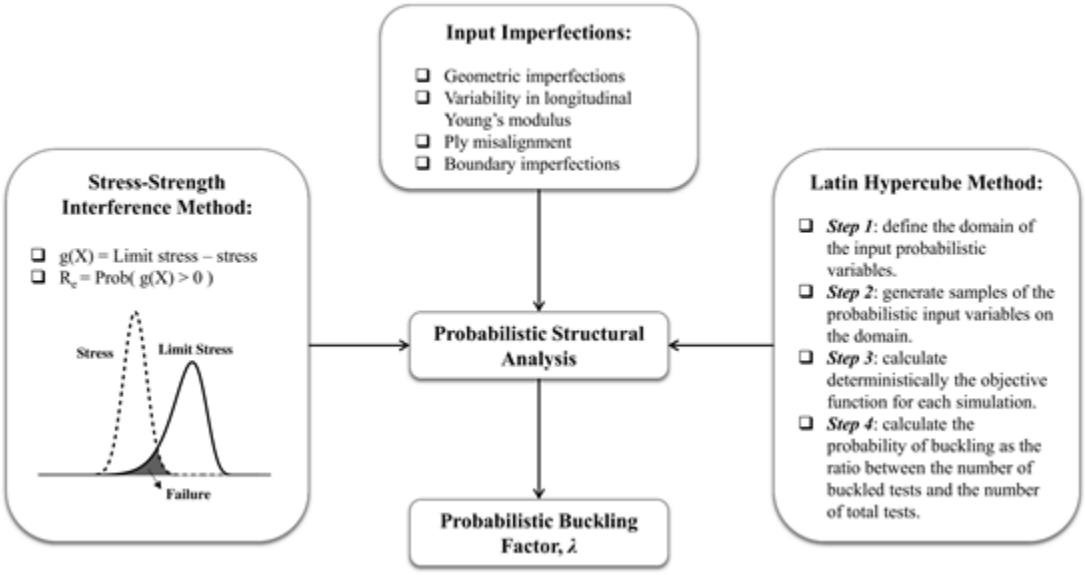

Figure 8. Block diagram of developed probabilistic procedure.

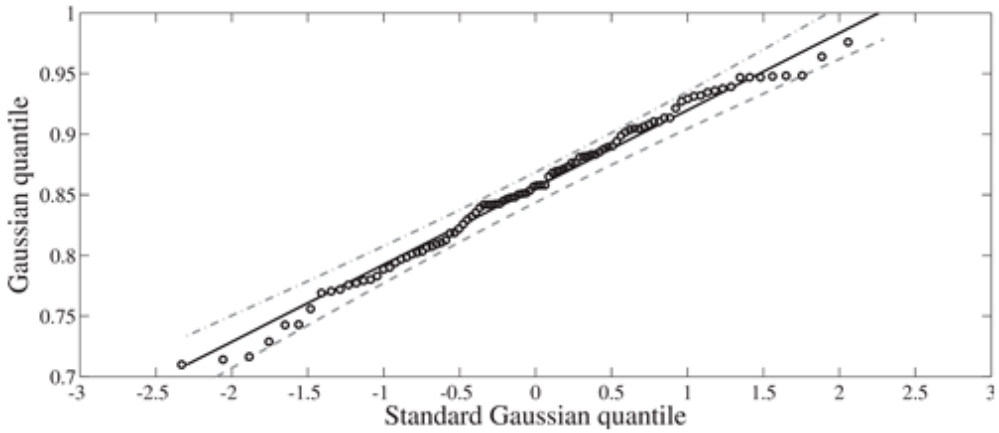

Figure 9. Quantile-quantile plot of data collection of $\Lambda_s(X)$ of SYLDA.

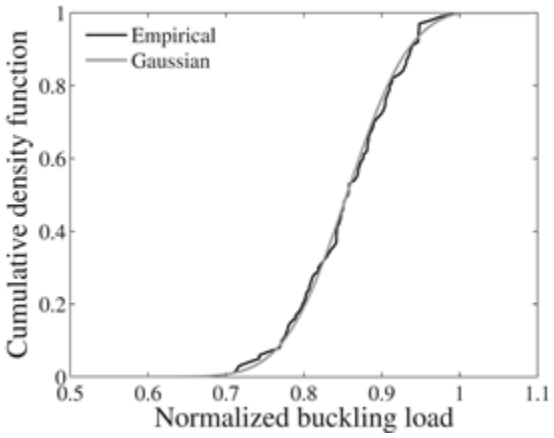

Figure 10. Empirical and Gaussian cumulative density functions of data collection of $\Lambda_s(X)$ of SYLDA.

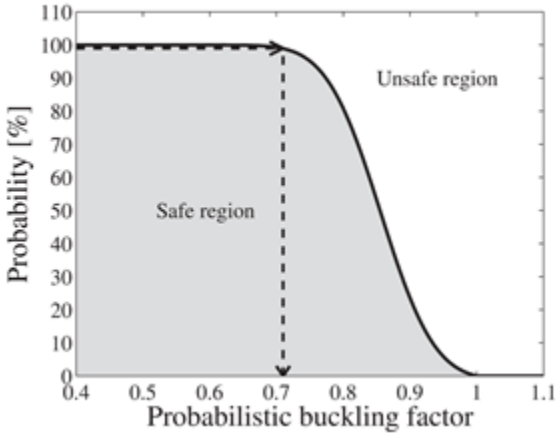

Figure 11. Probability $R_e(\lambda)$ that SYLDA does not buckle.

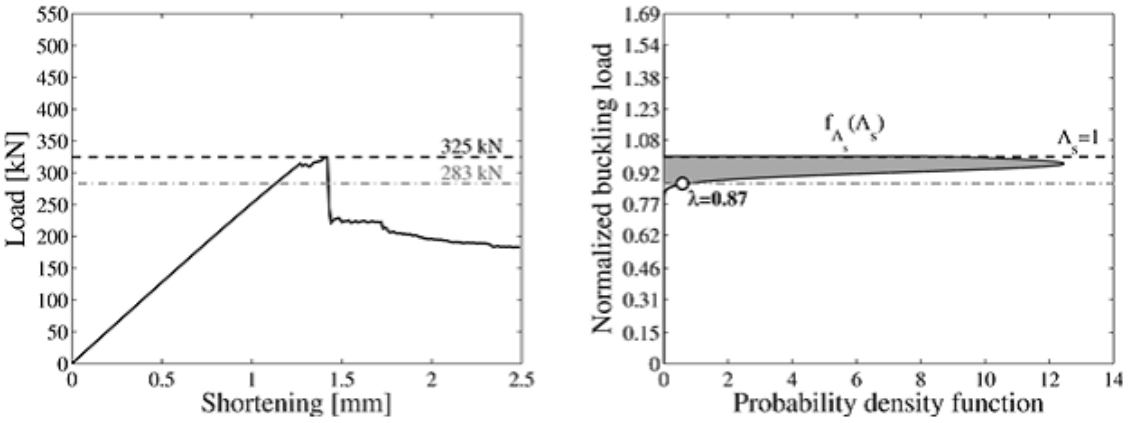

Figure 12. Load-shortening curve and distribution of $\Lambda_s(X)$ of SYLDA with cut-outs.

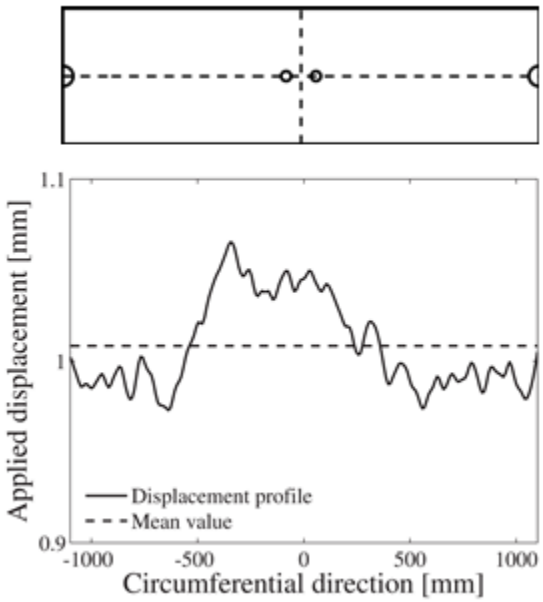

Figure 13. Non-uniform axial displacement applied to loaded edge of SYLDA with cut-outs.

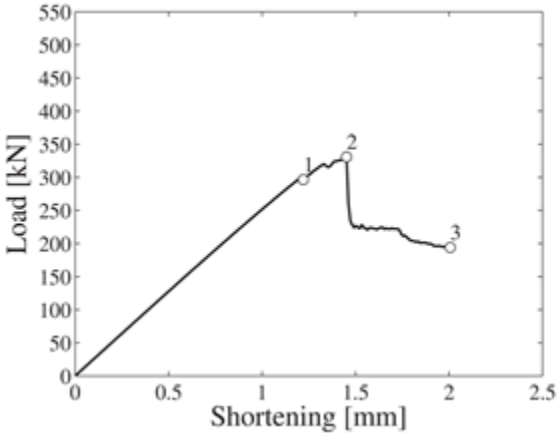

Figure 14. Load-shortening curve of SYLDA with cut-outs and boundary imperfections.

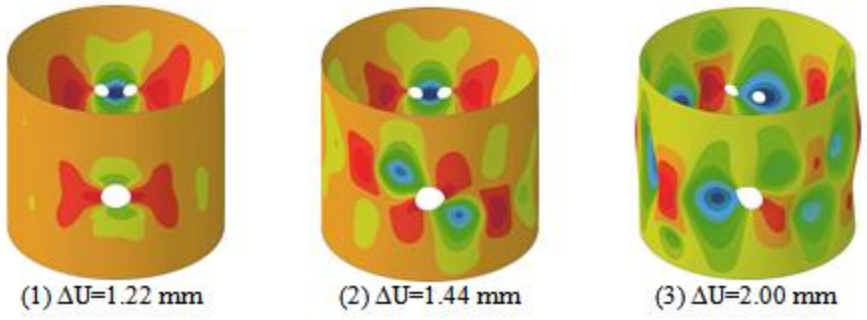

Figure 15. Deformed configurations for different imposed displacements ΔU of SYLDA with cut-outs and boundary imperfections.

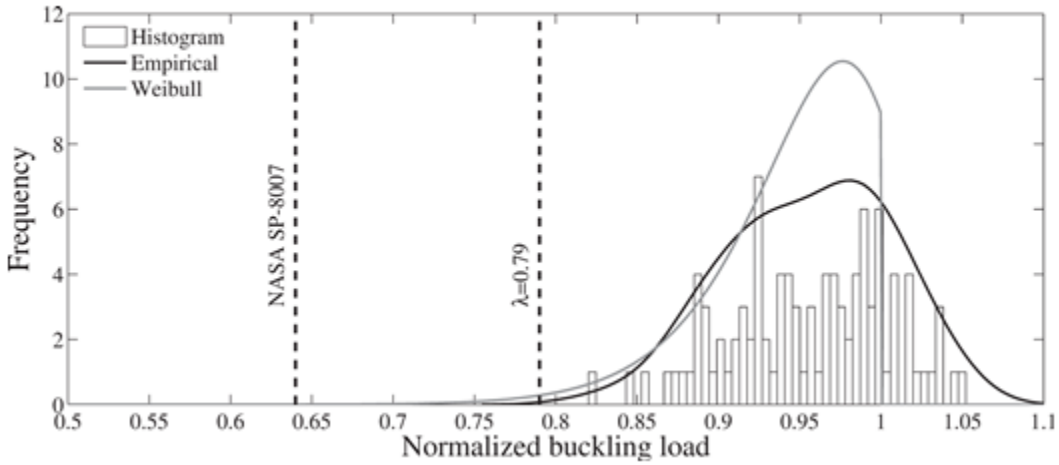

Figure 16. Histogram, empirical and Weibull probability density functions of data collection of $\Lambda_s(X)$ of ISS.